Quantifying hydrodynamic collective states of magnetic colloidal spinners and rollers

Y. Wang, S. Canic, G. Kokot, A. Snezhko, and I. S. Aranson

Phys. Rev. Fluids **4**, 013701 — Published 9 January 2019

DOI: 10.1103/PhysRevFluids.4.013701

Quantifying hydrodynamic collective states of magnetic colloidal spinners and rollers

Y. Wang[1], S. Canic[2,1], G. Kokot[3], A. Snezhko[3], I.S. Aranson[4]
[1] *Department of Mathematics, University of California, Berkeley, CA 94720*
[2] *Department of Mathematics, University of California, Berkeley, CA 94720*
[3] *Materials Science Division, Argonne National Laboratory, Argonne, IL60439*
[4] *Department Biomedical Engineering, Pennsylvania State University, University Park, PA16802*

Ferromagnetic micro-particles energized by an alternating magnetic field exhibit fascinating collective behavior ranging from the emergent self-assembled spinners to a variety of self-organized rolling states. Despite their simplicity, quantifying their essentially multi-body collective behavior remains elusive due to a multitude of relevant interactions, from short-range collisions to long-range magnetic and hydrodynamic forces. Here we develop a high-performance computational algorithm based on smoothed particle hydrodynamics to quantify the role of individual interactions in the emergent collective state. The computational model provides insight into the role of hydrodynamic interaction on the onset of collective behavior, and allows characterization of dynamic regimes that are hard to access experimentally. Comparison with high-resolution experimental data allows validation of the algorithm. Our work expands the scope of modern computational tools for predictive modeling of microscopic active systems, and provides insight into the intricate role of hydrodynamic interactions on the onset of collective behavior in living and synthetic active matter.

I. INTRODUCTION

Suspensions of driven microscopic solid particles, or colloids, represent an important and technologically relevant class of out-of-equilibrium systems. Their emergent behavior is governed by a multitude of forces, from steric collisions, gravity, friction, van der Waals, to long-range magnetic and hydrodynamic interactions [1, 12]. Due to the relative simplicity and ease of performing experiments, magnetic colloids energized by alternating magnetic field constitute a unique experimental system that led to a discovery of fascinating emergent collective behaviors, from self-assembled swimmers, microrobots, and spinners, to flocks, unstable fronts, etc [6, 13, 15, 17, 33, 35, 36, 40].

Recent studies highlighted close relations between the colloids driven by external electric or magnetic fields [3, 4, 13, 15, 17] and a broad class of non-equilibrium systems termed active matter: assemblies of self-propelled particles transducing stored energy into mechanical motion, such as bacterial swarms, cytoskeletal extracts, bird flocks, fish schools, etc [23, 31, 32, 38, 42]. The striking similarity between collective states in biological and inanimate matter, such as vortices, densification fronts, etc, suggests that the studies of driven colloidal systems may provide valuable insights into the behavior of their living counterparts.

Recently, we have observed the emergence of spinning [17] and rolling collective states [13, 18] of ferromagnetic colloids energized by a uni-axial alternating magnetic field. The colloids were either suspended at the air-water interface, or settled on the bottom of a container. Application of the magnetic field parallel to the interface resulted in self-assembly of spinning magnetic chains, and the onset of active turbulence [15, 17]. In contrast, the magnetic field applied perpendicular to the interface forced spinning particles to roll and form flocks and vortices [13]. In both cases, the steady spinning and rolling of particles emerge as a result of spontaneous symmetry breaking of particle rotations in a uniaxial alternating (AC) field. The symmetry-breaking takes place only in a certain range of the excitation field parameters. Since the uni-axial AC field can be decomposed into clockwise (CW) and counterclockwise (CCW) rotating fields, particle inertia results at the onset of rotation. Unlike in experiments reported in [6], the sense of rotation is not predetermined by the field, and it depends on the initial state of the particle.

A variety of numerical methods were used to understand the behavior of driven colloidal systems, from discrete particle dynamics [13, 17], to coarse-grained hydrodynamic methods [15] based on the multi-particle collision dynamics (MPCD) approaches [9, 22], or lattice-Boltzmann methods (LBM) [16, 37]. While simulations based on discrete particle dynamics are fast, they do not necessarily capture the relevant hydrodynamic interaction between the colloids. In contrast, MPCD and LBM simulations resolve the hydrodynamic interactions well, and lead to a much better agreement with experiment [15, 16]. Different numerical methods have different advantages and disadvantages, and their optimal performance may depend on the problem at hand. For example, the LBM are intrinsically stochastic and may require averaging over the noise. The MPCD is a particle-based mesoscale simulation technique for complex fluids, which is based on solving for the particle motion in one step, the streaming step, and then resolving particle collision in the collision step. While the MPCD method preserves the conservation of linear momentum, the conservation of angular momentum is not guaranteed due to its formulation. In scenarios when the hydrodynamics torque plays an important role, it may be a source of the discrepancy. Furthermore, the Reynolds number (Re) associated with the collective flocking state is of the order of 50 [13]. Thus, highly efficient hydrodynamic algorithms based on the solution of linear Stokes equation are not applicable. An efficient three-dimensional approach is needed to solve the finite Reynolds number Navier-Stokes equations with multiple solid inclusions.

For this purpose, we develop a high-performance computational algorithm based on a coarse-grained hydrodynamics simulation technique termed Smoothed Particle Hydrodynamics (SPH). The SPH was first proposed for solving astrophysics problems, and was later adapted for problems in fluid dynamics and solid mechanics. Over the last two decades, further development and improvement of the SPH method has allowed exploring a wider class of systems in incompressible flows, fluid-solid interaction, and solid mechanics [25–28]. As a mesh-free weighted interpolation method, the SPH is especially effective for complex multi-physics problems with large domain distortions [19]. In contrast with the mesh-based methods such as MPCD and LBM, the SPH does not rely on any fixed computational grid. Thus, the SPH can easily handle fluid mechanics problems involving free surface, wave breaking, and rapid geometry distortion. The SPH dramatically streamlines the procedures of numerically solving Navier-Stokers equations. Firstly, the SPH simplifies the nature of the Navier-Stokes equations since it is a Lagrangian method and non-linear convective terms in the Navier-Stokes equations disappear. Secondly, the momentum and energy equations could be solved explicitly in time, and there is no need to invert large linear systems. Finally, the pressure is directly computed from the equation of state for both gas and liquid phases, as the pressure depends on density only [20].

This is different from another popular grid-free coarse-grained simulation technique, the Dissipative Par-

ticle Dynamic (DPD) [7, 10], which is based on integrating out the internal, microscopic degrees of freedom, and relating them to simplified pairwise dissipative and random forces, providing local momentum conservation.

The SPH approach, proposed here, however provided faster and more efficient simulations which approximated well the experimental results. In particular, we faithfully reproduced experimentally observed frequency dependence of the roller speed, spatial structure of the vortex, and even 3D signature of the flow above the vortex. Comparison of the simulation results with high-resolution experimental data provided careful validation of the algorithm. It allowed elucidating a nontrivial role of the hydrodynamic interaction on the onset of collective motion, and allowed characterization of dynamic regimes that are hard to access experimentally. The validated algorithm can be readily applied to other colloidal systems, such as Quincke rollers [4], driven filament systems [31, 38], and may become a valuable tool for characterization of living and synthetic active matter.

II. DESCRIPTION OF THE COMPUTATIONAL MODEL

The computational approach is based on a coupled fluid-structure interaction algorithm implemented within the SPH framework. The Navier-Stokes equations for an incompressible, viscous liquid are used to model the fluid, while Newton equations for rigid particle motion are used to model the ferromagnetic colloids. The forces in the particle equations of motion include dipole-dipole magnetic particle interaction, and steric particle-particle repulsion. The impact of hydrodynamic forces is taken into account via explicit two-way coupling between the fluid and ferromagnetic particles, modeling continuity of velocity between the particles and fluid, and balance of contact linear and angular momenta.

A. The fluid equations

To model the fluid, we consider the Navier-Stokes equations for an incompressible, viscous Newtonian fluid in the Lagrangian framework:

$$\rho\frac{d\boldsymbol{v}}{dt} = -\nabla p + \mu_f\Delta\boldsymbol{v} + \rho\boldsymbol{g},$$
$$\nabla\cdot\boldsymbol{v} = 0,$$

where the notation for the total (Lagrangian) derivative d/dt corresponds to $\frac{d}{dt} = \frac{\partial}{\partial t} + \boldsymbol{v}\cdot\nabla$. Here ρ denotes the fluid density, $\boldsymbol{v}$ is the fluid velocity, p is the pressure, $\boldsymbol{g}$ is the gravity acceleration, and μ_f is the dynamic viscosity. To simulate incompressible fluid using the SPH (water in our study), we use a weakly compressible formulation, suggested in [26, 28]. The approach in [26, 28] is based on replacing the divergence free condition with the full conservation of mass equation in Lagrangian formulation:

$$\frac{d\rho}{dt} = -\rho\nabla\cdot\boldsymbol{v},$$

and using the following equation of state:

$$p(\rho) = p_0\Big[\big(\frac{\rho}{\rho_0}\big)^{\gamma} - 1\Big], \text{ with } p_0 = \frac{\rho_0 c^2}{\gamma}. \tag{1}$$

Here ρ_0 is the reference density, parameter γ is set to be 7 for water, p_0 is reference pressure, and c is artificial sound speed [28]. This gives rise to the following system of fluid flow equations:

$$\frac{d\rho}{dt} = -\rho\nabla\cdot\boldsymbol{v}, \tag{2}$$
$$\rho\frac{d\boldsymbol{v}}{dt} = -\nabla p + \mu_f\Delta\boldsymbol{v} + \rho\boldsymbol{g}, \tag{3}$$

supplemented with the equation of state (1). The incompressibility condition is well approximated as long as the colloids' speed is small relative to the artificial sound speed c [28].

B. Colloidal particle dynamics

1. 2D colloidal system driven by uniaxial in-plane alternating magnetic field

To calibrate the model and compare it with other techniques [15], we first considered ferromagnetic colloids dispersed in a thin layer of deionized water and suspended at air-liquid interface [17]. The particles were energized by a uniform uniaxial in-plane alternating magnetic field $H = H_0 \sin(\omega t)$, as shown in Fig. 1(a). As the energy injection rate varies, the ferromagnetic colloids self-assemble into a variety of 2D structures that range from pulsating clusters and wires, to dynamic arrays of spinners, as we show below in Sec. III A.

The dynamics of ferromagnetic colloidal particles is governed by the following equations

$$m\frac{d^2\boldsymbol{r}_i}{dt^2} = \boldsymbol{F}_i, \tag{4}$$

$$I\frac{d^2\phi_i}{dt^2} = T_i + \mu H_0 \sin(\omega t)\sin(\phi_i), \tag{5}$$

where $\boldsymbol{r}_i$ and ϕ_i stand for the particle position and orientation, respectively, m is the particle mass, μ is its magnetic moment, I is the moment of inertia, and $\boldsymbol{F}_i$ and T_i are the forces and torques arising from the magnetic field and particle interactions, specified in (8)-(9) below, and from the hydrodynamic forces due to fluid-structure interaction, described in Sec. II B 3. Since this problem is 2D, only the in-plane components of the forces and the normal component of the torque specified in (8)-(9) are considered.

A version of this model was first considered in Ref. [17] to study the emergent behavior of ferromagnetic colloids subject to an alternating magnetic field. However, in Ref. [17], the hydrodynamic forces due to fluid-particle interaction were modeled through approximations of fluid drag via the extra terms $\alpha_t\left(d\boldsymbol{r}_i/dt - \boldsymbol{V}_i\right)$ in equation (4), and $\alpha_r d\phi_i/dt$ in equation (5), where α_t and α_r are the translation and rotation drag coefficients, and $\boldsymbol{V}_i$ is the fluid advection velocity. In the present work, we take into account the hydrodynamic forces through a two-way fluid-structure coupling, as described in Sec. II B 3.

2. 3D colloidal system driven by a vertical AC magnetic field

We consider a 3D problem consisting of ferromagnetic colloids settled at a slightly concave bottom of a fluid container, subject to a vertical AC magnetic field $\boldsymbol{H}$, as illustrated in Fig.1 (b). This is in contrast with the previously considered 2D system, where the ferromagnetic colloids were energized by an in-plane AC magnetic field, and suspended at the 2D air-water interface. This problem is three-dimensional, and the application of AC magnetic field in vertical direction gives rise to new behaviors, including the emergence of flocking and global rotation [13].

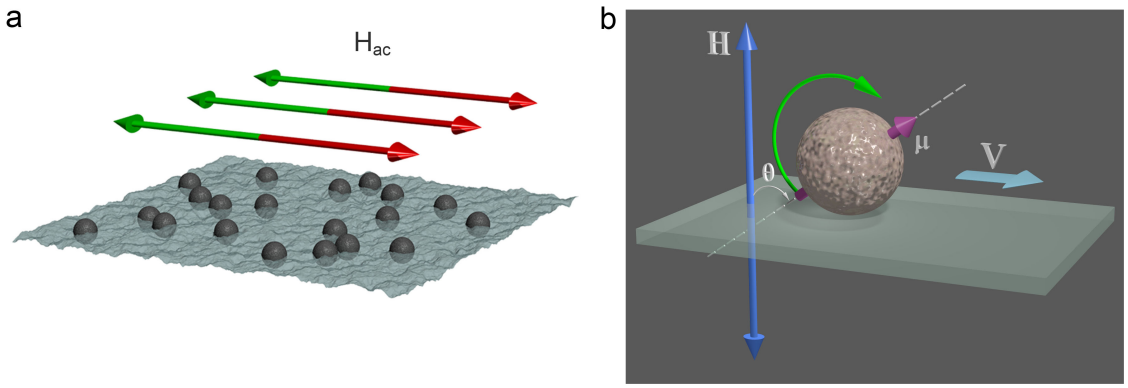

FIG. 1. Schematics of the experimental setups: (a) 2D scenario: Magnetic floaters suspended at water-air interface, energized by an in-plane AC magnetic field [17], and (b) 3D scenario: Magnetic rollers at the bottom of a concave container, energized by a vertical AC magnetic field [13].

To examine its behavior, we introduce a fluid-structure interaction model, which is based on a simplified discrete particle model from [13]. Instead of modeling the hydrodynamic forces based on their leading order

effective behavior, we model the fluid-structure interaction coupling explicitly. Notation $\boldsymbol{\Omega}_i$ is used to denote the angular velocity w.r.t the x, y, and z axis. Vector $\boldsymbol{n}_i$ denotes the unit normal to the bottom surface at the position of particle i, i.e, a unit vector pointing from the colloid contact point with the surface to its center of mass. As before, $\boldsymbol{F}_i$ and $\boldsymbol{T}_i$ are the forces and torques due to the magnetic dipole-dipole interaction and hard-core repulsions, specified in (8)-(9). In contrast with Ref. [13], we also include the hydrodynamic forces due to fluid-structure interaction, as specified in Sec. II B 3.

$$m\frac{d^2\boldsymbol{r}_i}{dt^2} = \boldsymbol{F}_i, \tag{6}$$

$$I\frac{d\boldsymbol{\Omega}_i}{dt} = \boldsymbol{T}_i + \boldsymbol{\mu}_i \times \boldsymbol{H}, \tag{7}$$

where m is the particle mass, $\boldsymbol{\mu}_i = \mu\hat{\boldsymbol{u}}_i$ is its magnetic moment with $\hat{\boldsymbol{u}}_i$ denoting the corresponding unit vector, I is the moment of inertia. $\boldsymbol{F}_i = \sum_j \boldsymbol{F}^D_{i,j} + \sum_j \boldsymbol{F}^H_{i,j} + \boldsymbol{F}^C_i + \boldsymbol{F}^F_i$ is the total force on the i-th particle given as a sum of forces due to dipole-dipole interaction $\boldsymbol{F}^D_{i,j}$, hard-core repulsion (steric forces) $\boldsymbol{F}^H_{i,j}$, curvature of the bottom $\boldsymbol{F}^C_i$, and fluid-particle interaction coupling $\boldsymbol{F}^F_i$. Similarly, $\boldsymbol{T}_i = \sum_j \boldsymbol{T}^D_{i,j} + \boldsymbol{T}^F_i$ are the corresponding torques. They are given by the following:

- The dipole-dipole interaction gives the following force exerted by colloid i on colloid j [13]:

$$\boldsymbol{F}^D_{i,j}(\boldsymbol{r}, \hat{\boldsymbol{u}}_i, \hat{\boldsymbol{u}}_j) = \frac{3\mu}{4\pi|\boldsymbol{r}|^4}(\hat{\boldsymbol{u}}_j(\hat{\boldsymbol{u}}_i \cdot \boldsymbol{r}) + \hat{\boldsymbol{u}}_i(\hat{\boldsymbol{u}}_j \cdot \boldsymbol{r}) + \boldsymbol{r}(\hat{\boldsymbol{u}}_i \cdot \hat{\boldsymbol{u}}_j) - 5\boldsymbol{r}(\hat{\boldsymbol{u}}_i \cdot \boldsymbol{r})(\hat{\boldsymbol{u}}_j \cdot \boldsymbol{r})), \tag{8}$$

  where $\boldsymbol{r}$ is the unit vector pointing from colloid i to j. The force acting on colloid i is in the opposite direction. Vector $\hat{\boldsymbol{u}}_i$ is the unit vector in the direction of the magnetic moment of colloid i, with the magnetic moment given by $\boldsymbol{\mu}_i = \mu\hat{\boldsymbol{u}}_i$.

- Steric hard core repulsion force $\boldsymbol{F}^H_{i,j}(\boldsymbol{r}) = -\nabla U^H_{ij}$ is derived from stiff interaction potential $U^H_{ij} = \frac{\mu^2}{16\pi a^3}(\frac{a}{r_{ij}})^{24}$.

- Force $\boldsymbol{F}^C_i(\boldsymbol{r}) = -\nabla U^C_i$ coming from the harmonic potential $U^C_i = \kappa r_i^2$ due to bottom curvature.

- The dipolar magnetic torque exerted by particle i on particle j is of the form:

$$\boldsymbol{T}^D_{i,j} = \hat{\boldsymbol{u}}_i \times \boldsymbol{B}_j = \hat{\boldsymbol{u}}_i \times \Big[\frac{\mu_0}{4\pi|\boldsymbol{r}|^2}\big(\frac{3\boldsymbol{r}(\hat{\boldsymbol{u}}_j \cdot \boldsymbol{r})}{|\boldsymbol{r}|^2} - \hat{\boldsymbol{u}}_j\big)\Big]. \tag{9}$$

The hydrodynamnic force and torque due to fluid-particle interaction are specified below.

3. *The fluid-particle interaction coupling*

Two-way coupling between fluid and colloidal particles is described by the no-slip condition (kinematic coupling) and by the balance of contact stresses/traction (dynamic coupling) on particle surface.

Kinematic coupling: The no-slip boundary condition enforces continuity of velocities between the fluid and particle on the particle surface. For colloid i, the no-slip condition states

$$\boldsymbol{v}|_{\gamma_i} = \boldsymbol{V}_i, \tag{10}$$

where γ_i denotes the boundary (surface) of particle i, $\boldsymbol{v}|_{\gamma_i}$ is the trace of the fluid velocity on γ_i, and

$$\boldsymbol{V}_i = \boldsymbol{V}^t_i + \boldsymbol{V}^r_i = \boldsymbol{V}^t_i + \boldsymbol{\Omega}_i \times \boldsymbol{r},$$

is the velocity of the rigid particle i, which consists of two components: the translational velocity $\boldsymbol{V}^t_i$, and the rotational velocity $\boldsymbol{V}^r_i = \boldsymbol{\Omega}_i \times \boldsymbol{r}$, where $\boldsymbol{r}$ is the radius vector of the rigid particle, $\|\boldsymbol{r}\| = a$. Through this condition, the fluid "feels" the motion of the particle. In the SPH framework, a colloidal particle of radius a is represented by several SPH particles, which satisfy different equations of motion than the SPH fluid particles away from the colloid. In particular, the SPH particles that belong to the interior and to the surface of the colloid are updated according to rigid body rotation:

$$\boldsymbol{V}_{i,j} = \boldsymbol{V}^t_i + \boldsymbol{\Omega}_i \times (\boldsymbol{r}_{i,c} - \boldsymbol{r}_{i,j}), \qquad \text{for} \quad \|\boldsymbol{r}_{i,c} - \boldsymbol{r}_{i,j}\| \le a,$$

where $\boldsymbol{r}_{i,c} - \boldsymbol{r}_{i,j}$ is the vector pointing from the center of the rigid particle i to a SPH particle $\boldsymbol{r}_{i,j}$ located within the radius a from the center of the rigid particle i. Note that the fluid SPH particles that lie on the colloid surface within the radius a around the center of particle i obey the no-slip condition.

Dynamic coupling: The dynamic coupling states that the traction force that the particle "feels" on its surface is the fluid normal stress (contact force): $\boldsymbol{\tau} = \boldsymbol{\sigma}\boldsymbol{n}|_{\gamma_i}$. Therefore, the equations of motion for particle i will have contributions from the hydrodynamic force $\boldsymbol{F}_i^F$ and torque $\boldsymbol{T}_i^F$, given by:

$$\boldsymbol{F}_i^F = -\int_{\gamma_i} \boldsymbol{\tau} d\gamma_i = -\int_{\gamma_i} \boldsymbol{\sigma}\boldsymbol{n} d\gamma_i,$$
$$\boldsymbol{T}_i^F = -\int_{\gamma_i} (\boldsymbol{r}_{i,c} - \boldsymbol{r}_{i,a}) \times \boldsymbol{\tau} d\gamma_i = -\int_{\gamma_i} (\boldsymbol{r}_{i,c} - \boldsymbol{r}_{i,a}) \times \boldsymbol{\sigma}\boldsymbol{n} d\gamma_i,$$

where $\boldsymbol{r}_{i,a}$ denotes the fluid particles at distance a from the center of particle i, i.e., the fluid particles in contact with the particle surface γ_i.

This is implemented in the SPH algorithm by approximating the surface integrals via summation over the fluid particles at distance a from the center of the colloid i:

$$\boldsymbol{F}_i^F = -\sum_{\boldsymbol{r}_{i,a} \in \gamma_i} \boldsymbol{\sigma}\boldsymbol{n}, \qquad \boldsymbol{T}_i^F = -\sum_{\boldsymbol{r}_{i,a} \in \gamma_i} (\boldsymbol{r}_{i,c} - \boldsymbol{r}_{i,a}) \times \boldsymbol{\sigma}\boldsymbol{n}. \tag{11}$$

Additional details on the implementation of the SPH algorithm and on the validation of the model can be found in Supplementary Material [2, 5, 8, 11, 14, 19–21, 24–30, 39, 41].

III. RESULTS

A. Two-dimensional simulations: self-assembled spinners and wires

The SPH approach, described above, was used to capture $2D$ dynamics of self-assembled wires and spinners at the water-air interface. An alternating external magnetic field $H = H_0 \sin(2\pi f t) = H_0 \sin(\omega t)$ with the frequency f and amplitude H_0 was applied parallel to the surface. The magnetic field energizes the system by exerting torques on the particles. The torques are dissipated locally in the liquid as they generate fluid flow around the particles [17]. Consequently, the particles interact by two major forces: magnetic (dipole-dipole interactions) and hydrodynamic. Depending on the frequency and amplitude of the magnetic field, different phases were observed in experiments [17], including spinners and wires, as shown in Fig. 2.

The model presented in Sec. II B 1 was used to simulate the colloids. A total of 6000 particles was used in our simulation, with the ratio of colloids to fluid particles of 1 : 10. We note that this ratio is higher than that used in [15]. The colloidal particles are initially distributed randomly. The values of the coefficients used in the simulations are presented in Table I, Sec. IV: Methods. The simulation time step is dependent on the frequency f of the magnetic field, and is equal to $\Delta t = \frac{1}{16 \times f}$.

Figure 2 shows a comparison between the experiment [17] and numerical simulations. The frequency and amplitude of the magnetic field are $f = 50$ Hz and $H_0 = 25$ Oe for the spinners, and $f = 150$ Hz and $H_0 = 25$ Oe for the wires. These values correspond to the parameter values for which spinners and wires were obtained in the experiment [17]. The plots (a) and (b) in Fig. 2 show streamlines of fluid velocity field at the air-liquid interface in experiment and numerical simulation, respectively, for the spinner phase. Particle-image velocimetry was used to create the plot showing experimental result in (a). The SPH method described above was used to create the plot showing computational results in (b). One can observe similarity in vorticity fields, typically associated with the spinner phase, in which an assembly of two or more particle spins and creates local vortices. The plots in (c) and (d) show the magnitude of fluid velocity generated by the spinners. Again, qualitatively similar behavior between experiment (c) and simulation (d) can be observed. The plots (e) and (f) illustrate the spinners and wires, respectively. The particles are shown in red, superimposed over the velocity vector field, shown in grey. We observed that in the spinner phase, the spinners rotate clock-wise or counter clockwise with equal probability. Therefore, we adopted the approach from [17] to examine the order parameter for spinner imbalance. The spinner imbalance parameter is defined as $I = (N_+ - N_-)/(N_+ + N_-)$, where N_+ and N_- denote the number of clockwise and counterclockwise spinners respectively. Figure 3 (a) shows the spinner imbalance over 2000 periods.

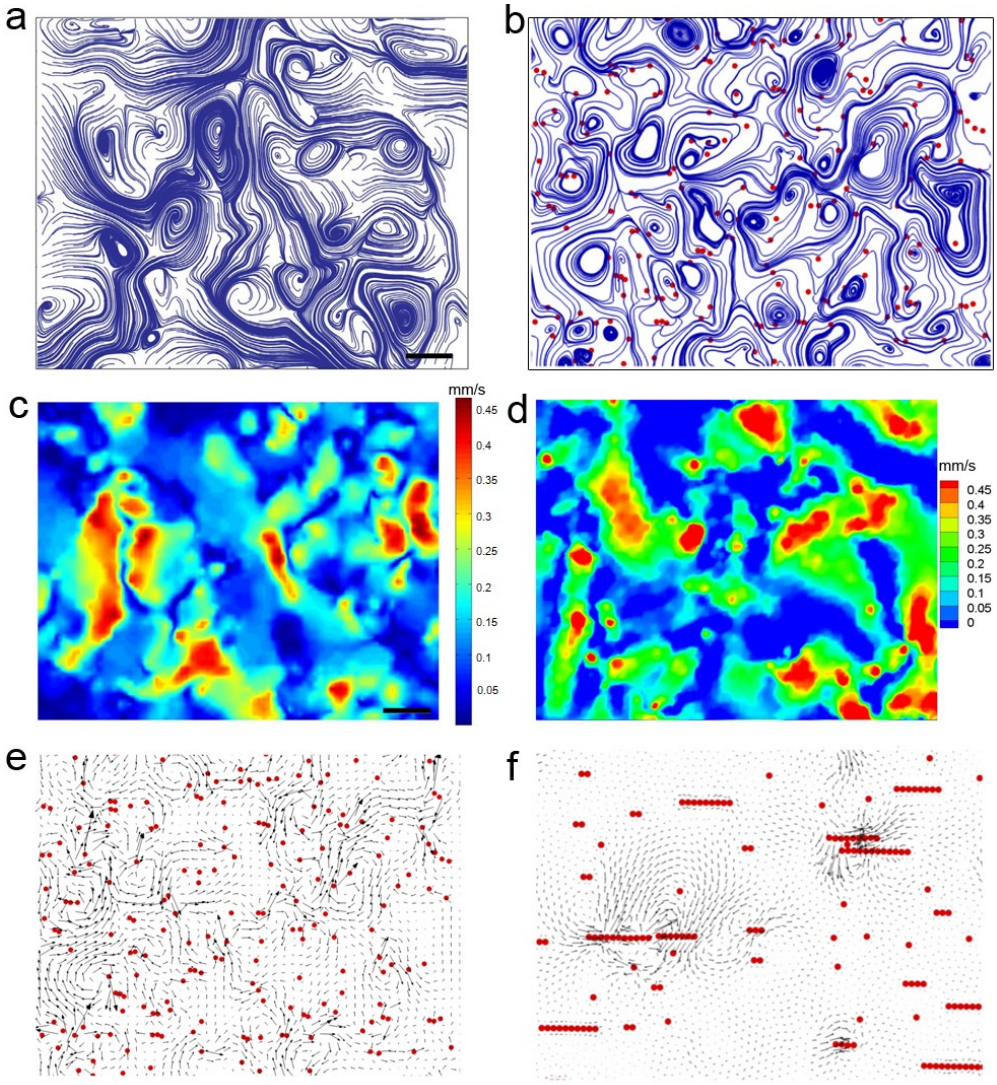

FIG. 2. Comparison of experiment [15, 17] and numerical simulations of the SPH model for 2D spinners and wires. Spinners: streamlines (experiment) (a); simulations (b); fluid velocity magnitude (experiment) (c) and simulations (d); (e) Spinners with the fluid velocity vectorfield, simulations; (f) Wires with the fluid velocity vectorfield, simulations.

We observe that the SPH results agree well with experiment, producing the same type of collective behavior for the same parameter values as in the experiment. Additionally, a comparison with the previous MPCD studies based on a simplified, effective model reported in [15], shows good agreement as well.

B. Three-dimensional simulations: rolling colloids

To quantify the effect of hydrodynamic forces due to fluid-particle interaction on the colloid motion, we first study the dynamics of an isolated colloid subjected to a vertical AC field. A single colloid is placed near the center of a flat, rectangular surface. The particle is immersed in the fluid, and energized by a vertical AC magnetic field. Neither dipole-dipole interaction nor gravitational potential force is present. The expected particle trajectory is a straight line. Figure 4 (a) shows the trajectory obtained from simulation. Indeed, as Figure 4 (a) shows, before the particle hits the wall, the particle path is close to a straight line. The wall interactions and the hydrodynamic forces induced by the fluid-particle interaction drive the colloidal particle away from the straight line. The plot in Figure 4 (b) shows a magnified view of the fluid velocity field near the particle. It has the signature of a hydrodynamic monopole. Since the flow generated by a monopole has

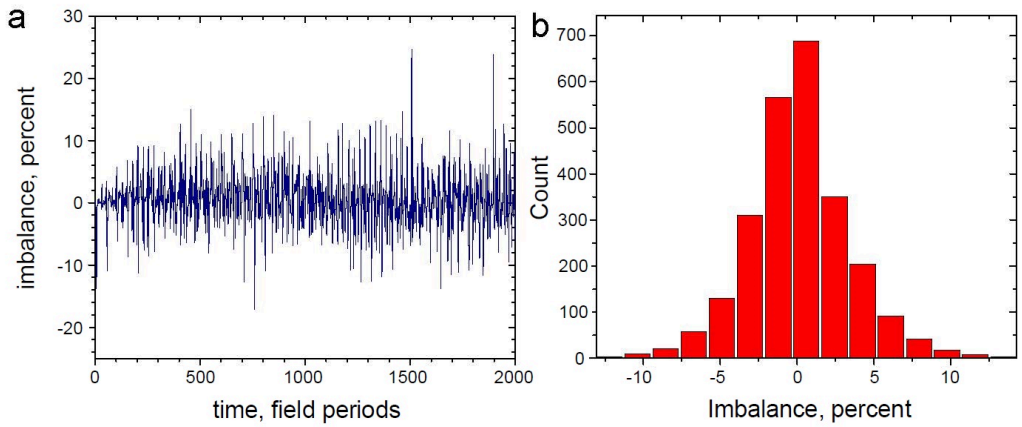

FIG. 3. Imbalance in the number of spinners with different sense of rotation as a function of time. Within the reported 2000 periods, the spinner imbalance parameter fluctuates significantly (a); Histogram of the spinner imbalance parameter values (b). Both plots indicate absence of directional synchronization between spinners.

a longer range of influence than that of a dipole, we anticipate that the hydrodynamic forces will dominate the dynamics of many colloids as well, thereby emphasizing the need for careful resolution of fluid-particle interactions.

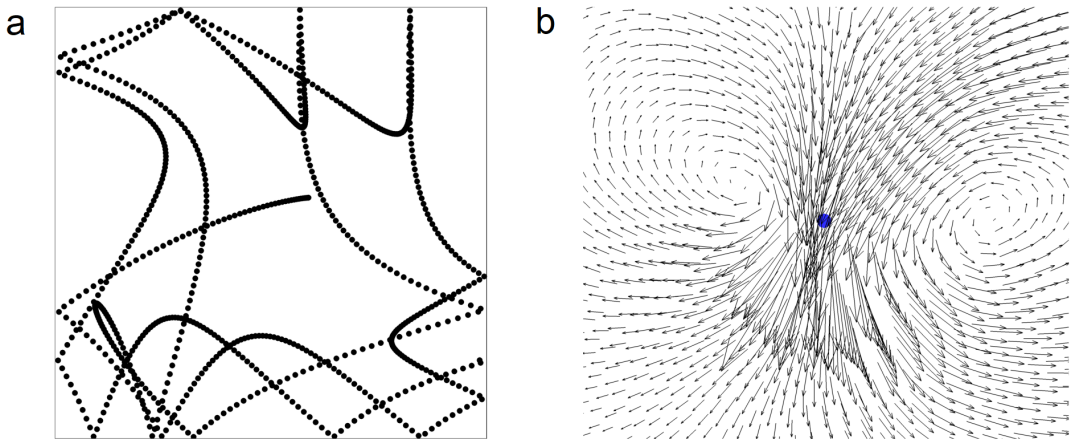

FIG. 4. Single particle trajectory (a), and fluid velocity vector field generated by a single particle (b).

Next, we investigate the emergence of collective states in a system of rolling ferromagnetic micro-particles. The particles are randomly distributed at the bottom of a slightly concave lens in a shallow layer of water covering the particles, and energized by a vertical AC magnetic field. The experimental investigation of the emergent behavior, presented in [13], showed that depending on the frequency and amplitude of the magnetic field, various collective behaviors appear, including a gas-like phase, flocking, and global rotation around the center of the lens, i.e., a 3D vortex.

The $3D$ computational model, presented in Secs. II B 2 and II B 3, was used to capture the phases observed in the experiment. The values of the coefficients in the model are shown in Table II in Sec. IV. Because full fluid-particle interaction was taken into account, our results provide detailed information about colloids' emergent behaviors, including spatial distribution of fluid flow. A total of 40,000 particles were used, 220 represented the colloids. At $t = 0$, the colloids were randomly distributed at the bottom of the surface. To simplify the calculations, we included the gravitational force rather than the SPH particles to recreate the curvature of the lens. A vertical AC magnetic field $\boldsymbol{H}$ was applied to energize the particles.

All the phases observed in experiments [13] were recovered computationally. Below we report the results obtained for three different values of magnetic field with frequencies (Hz) and magnitudes (Oe) equal to $(f, H_0) = (5, 20), (35, 50)$ and $(40, 50)$. The three cases correspond to the gaseous phase, flocking, and vortex, respectively.

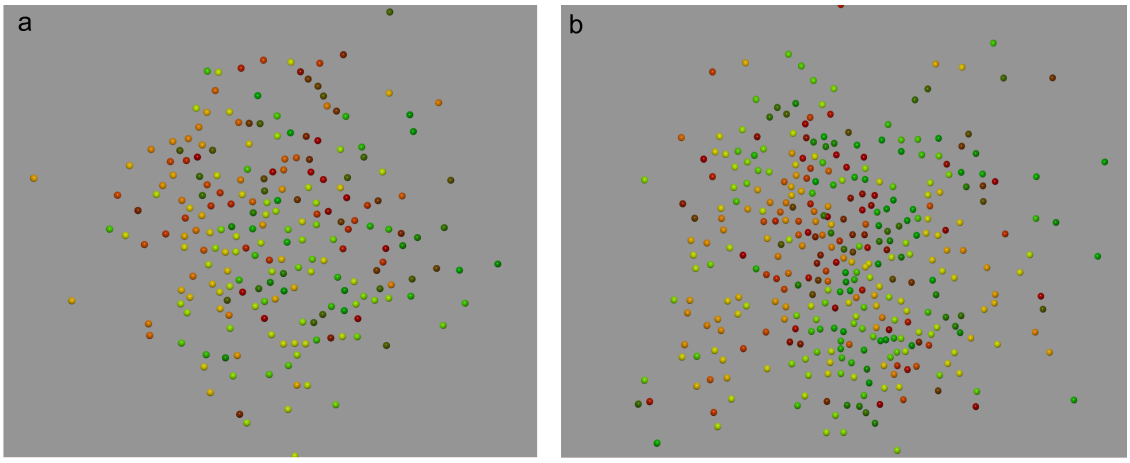

FIG. 5. Flocking behavior obtained in a system of magnetic rollers. The direction of particle motion was color-coded in visualization using the following rule: $[\text{red}, \text{green}, \text{blue}] = [(1+\sin(\varphi))/2, (1+\cos(\varphi))/2, 0]$, where φ is the angle of the in-plane velocity vector with respect to the x-axis. Thus, a group of particle with the same color identifies one flock. (a): computational results obtained for frequency $f = 35$ Hz and magnitude $H_0 = 50$ Oe. (b): experimental result for $f = 50$ Hz. One sees correlated motion of intermittent flocks of particles, illustrated by color patches.

Figure 5 shows the flocking phase. Panels (a) and (b) correspond to the computational and experimental results, respectively. The direction of particle motion was color-coded, as explained in the caption of Figure 5, so that color patches illustrate (correlated) flocking motion. Thus, intermittent formation of flocks appears both in experiments and in numerical simulation results.

Figure 6 shows the vortex phase, obtained with $f = 40$ Hz and magnitude $H_0 = 50$. Panels (a) and (b) depict the velocity field magnitude with the same color code to highlight the similarity between experimental and simulation results. Panel (b) also shows the velocity vector field, superimposed over velocity magnitude. Excellent agreement can be observed between experiment and simulation. This can be contrasted with the simulation results from [13], where hydrodynamic interactions were included only in the far-field approximation, and not through full fluid-particle interaction modeling. This simplification resulted in a large "void" region in the center of the vortex, which we do not observe in our simulations incorporating full hydrodynamic interactions.

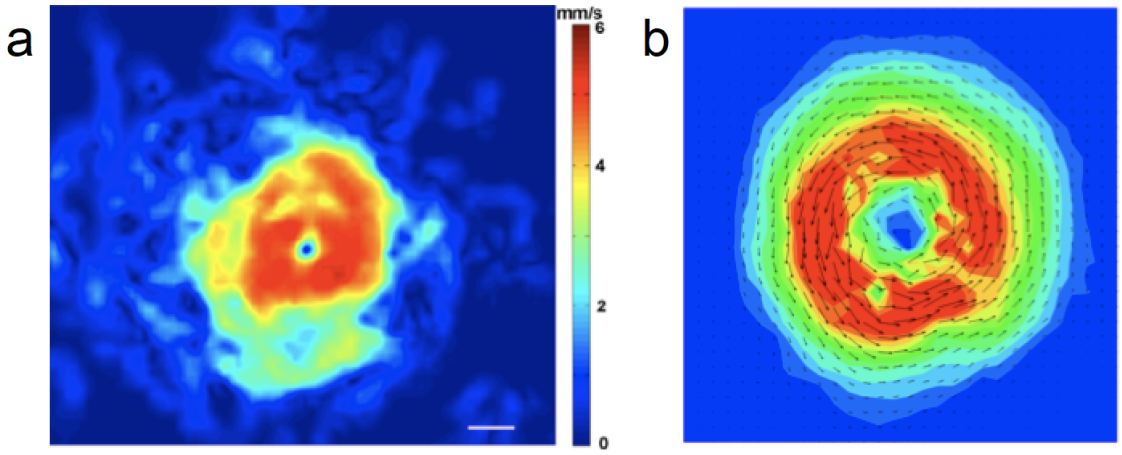

FIG. 6. Vortex obtained with the vertical AC magnetic field with frequency $f = 40$ Hz and magnitude $H_0 = 50$ Oe. (a): fluid velocity magnitude (experiment). (b): fluid velocity magnitude superimposed over the fluid vector field (computation).

For the vortex phase, we also compared the vortex velocity profile as a function of the distance from the center of rotation, see Fig.8 (a). Experimental and numerical results are shown in blue and gray dots and diamonds, respectively. One can see that both the simulation and experimental data show similar trend: the colloids' velocity is small near the center, it then increases and reaches it maximum around 5 mm/s near the effective vortex radius of around 0.7 mm, and then decreases with the increase in the distance from the center.

To characterize the self-generated surface hydrodynamic flows, we calculated the flow velocity spatial correlation function based on the fluid velocity data, as in Ref. [34]. Figure 7 (a) confirms long-range spatial correlations of the flow. Moreover, the correlation function shows oscillations characteristic to a large-scale vortex motion. This observation is in both qualitative and quantitative agreement with the experiment [13]. We also quantified the order parameter corresponding to in-plane rotational collective motion ϕ_R [13]. It is obtained by taking the normalized tangential components of velocities for all particles, and then averaging the tangential component of the velocity over the entire ensemble. The time evolution of the order parameters for three different phases is shown in Fig. 7 (b). The order parameter for the rotational collective motion of the gas state is around 0, indicating no collective motion. In the flocking state, the order parameter fluctuates around 0.24, indicating that the flocks are persistently assembling and dissembling. In the vortex state, the value is close to 1, which corresponds to pure rotation.

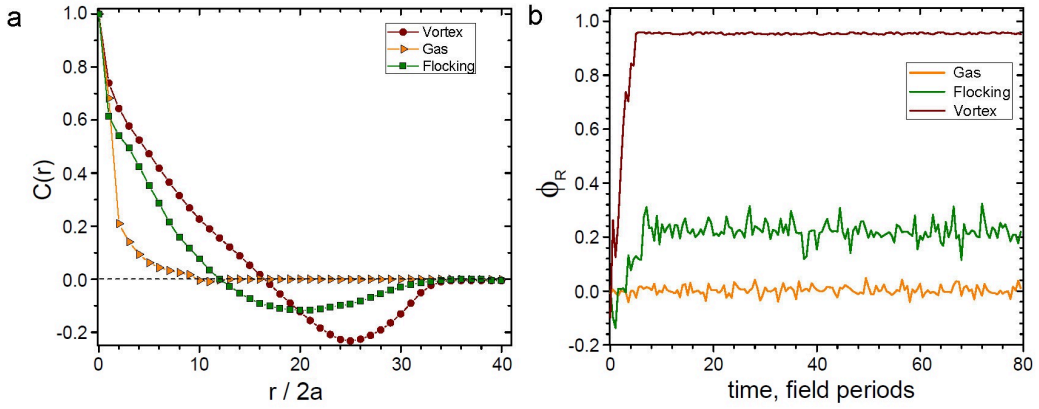

FIG. 7. (a) Velocity spatial correlation functions for different phases as obtained from simulations; a stands for the particle radius. (b) Rotational order parameter ϕ_R for different phases (simulations).

It has been observed experimentally [13] that the speed of rolling colloidal particles does not match to the expected speed calculated from the rollers diameter, and that there is a correction due to the slipping of particle against the bottom surface. The slipping is a consequence of the lifting force due to fluid-particle interaction. When the frequency of the external magnetic field exceeds a certain threshold, the lifting force may dominate the gravitational force and cause the colloids to have an upward motion. In Ref. [13], the slipping parameter α_s was obtained experimentally to be between 0.25 and 0.3, and was used as an *ad hoc* parameter in the simplified, effective equations of motion of colloids in [13] to simulate their dynamics. In the present work, due to the inclusion of fluid-particle interaction in the model, we do not use the *ad hoc* slipping term. Instead, our simulations produced the slipping of the colloids as a direct outcome of the model, with the correct slipping factor $\alpha_s \approx 0.25 \sim 0.3$. Figure 8 (b) shows the values of the slipping parameter α_s calculated from the simulations at different frequencies, and compared with the values of α_s obtained from experiment. We see excellent agreement between the these two. To further investigate the upward motion of colloids associated with the slipping, we recorded the vertical position of the center of mass of a randomly chosen particle over 200 periods of the driving frequency. A typical trajectory of the center of mass is shown in Fig. 9 (a). This figure explicitly shows significant lifting, which can be correlated with the observed slipping.

To fully investigate the vortex emergent behavior, full 3D distribution of flow velocity is desirable, but hard to obtain experimentally. For this purpose, we plot in Figure 9 (b) the streamlines of the fluid velocity field, and in Figure 9 (c) we show the density plot of the vertical velocity component in a cross-section through the vortex eye. Two interesting observations can be made: (1) the motion of the colloids causes the fluid locally to move upward and downward in a somewhat random fashion; and (2) the fluid forms a large

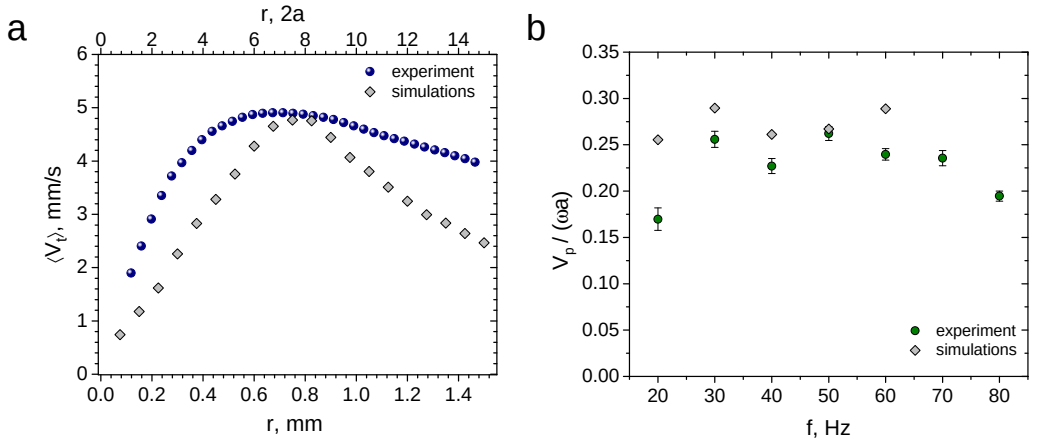

FIG. 8. (a) Comparison of the vortex velocity profiles versus distance from the center; solid line corresponds the experimental data, squares correspond the simulations. (b) Ratio between the peak velocity V_p and normalized particle velocity $V_0 = \omega a$, which is used to determine the slipping parameter α_s: experimental data is shown in diamonds, and simulation data in circles.

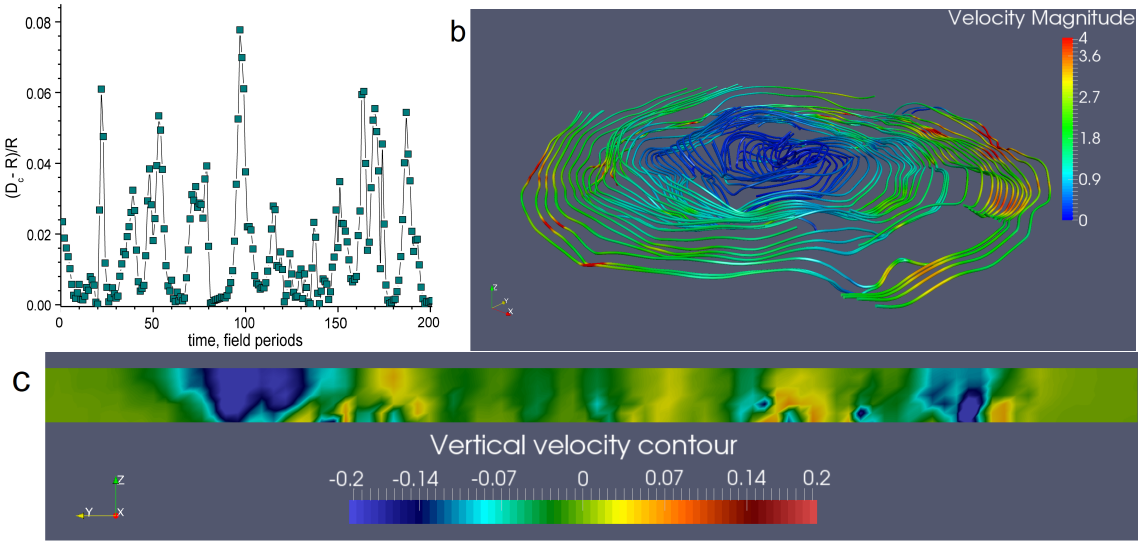

FIG. 9. (a) Vertical center of mass position of a colloidal roller vs time, D_c and R stand for the location and radius of a colloid respectively. (b) In -plane streamlines and (c) vertical cross-section of the fluid velocity field in the vortex phase. The cross-section is taken through the eye of the vortex.

vortex, which influences the colloids to move toward the vortex eye. This may explain the appearance of the region devoid of particles near the vortex eye, which was reported in [13], and obtained using the simplified mathematical model. The lack of detailed modeling of hydrodynamic interactions in Ref. [13] results in particle rolling away from the vortex center.

In addition, Figure 10 shows the time evolution of the particles center of mass for the vortex. The blue and red curves correspond to the x and y coordinate of the vortex center of mass versus time. Panel (a) corresponds to the experiment, and panel (b) to the numerical simulations. Similar patterns are observed: the vortex eye is oscillating with similar frequency in the experiment and simulations. Both, experiment and simulations indicate oscillations of the vortex eye position around the center of the harmonic confinement. Fourier analysis of the obtained simulation data reveals a pronounced peak in the spectra at about 0.22 Hz indicative of a characteristic oscillation frequency, see Fig. 10d. Similar analysis of the experimental data (panel c in Fig. 10) recovers the similar behavior. The spectral peak there is much boarder due to non-uniformity of the particles' sizes and shapes involved in the vortex. However, the peak position is remarkably close to the simulated value.

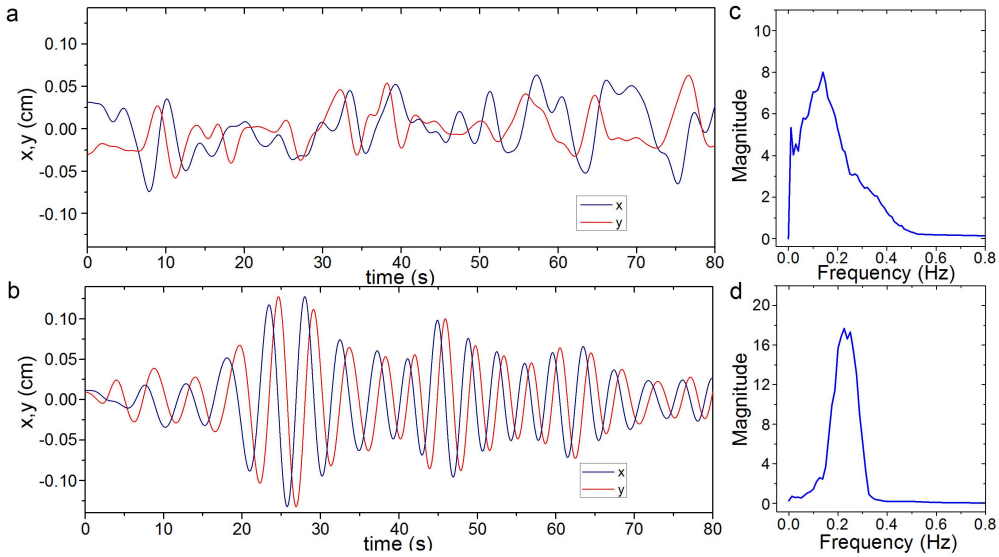

FIG. 10. Time evolution of the roller vortex horizontal center of mass: (a) experiment (b)simulations. Blue and red lines correspond to x and y components of vortex center of mass respectively. Fourier analysis of the vortex eye oscillations for experiment (c) and simulations (d).

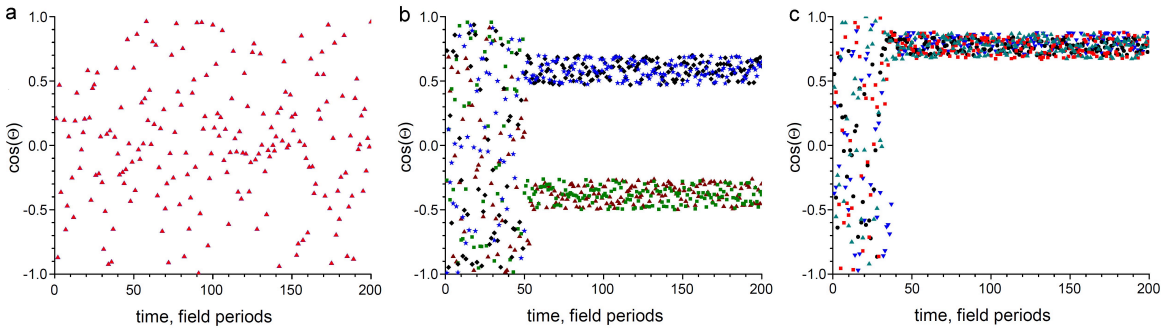

FIG. 11. The stroboscopic plots of the vertical components of colloids' magnetic orientation $\cos(\theta)$ in three different dynamic phases: The angle θ is the angle between the particle magnetic moments and the vertical direction. Different colors correspond to different (a) Gas; (b) Low-frequency flocking; (c) Vortex.

Onset of large-scale collective behavior. It was reported in [13] that the onset of large-scale collective behavior (spatial coherence) is correlated with the synchronization of particle orientation with the direction of the external AC magnetic field. To investigate the ability of our model in capturing the onset of large-scale collective behavior and transition between different phases, we calculated and plotted the stroboscopic particle orientation $\cos(\theta)$ for all the phases, and compared those values with that of Ref. [13]. We were able to recover the same behavior as in particle simulations [13]. In the gas-like phase, the magnetic moment orientation of the colloids is uniformly distributed and uncorrelated, see Fig. 11 (a). With the increase in frequency of the external magnetic field, the gas phase is transformed into the flocking phase. In the flocking phase the magnetic moment orientation of the colloids groups into two bands, which corresponds to two rotation directions: clockwise and counterclockwise rolling, see Fig. 11 (b). With a further increase in frequency, the magnetic moment orientation of the colloids converges to a single band for the vortex phase, as shown in Fig. 11 (c). This is exactly what is observed in Ref. [13]. We conclude that our model provides a reliable tool to capture the collective behavior of colloidal suspensions, both in terms of their structure, and in terms of correctly capturing the onset of different collective behaviors.

IV. METHODS

A. Computational model parameters

colloid diameter	$a = 75 - 100\mu m$	magnetic moment	$\mu = 2 \times 200\mu emu$
magnetic field amplitude	$H_0 = 10 - 60$ Oe	frequency	$f = 5 - 300$ Hz
moment of inertia	$I = \frac{2}{5}ma^2$		

TABLE I. Parameter values for 2D simulations

colloid radius	$a = 60\mu m$	magnetic moment	$\mu = 2 \times 10^{-5} emu$
lens radius of curvature	$r_c = 52$ mm	lens diameter	$r = 50$ mm
magnetic field amplitude	$H_0 = 0 - 75$ Oe	frequency	$f = 5 - 60$ Hz
moment of inertia	$I = \frac{2}{5}ma^2$		

TABLE II. Parameter values for 3D simulations

B. Experimental Settings

Experiments with magnetic rollers were performed in a cylindrical container with a concave bottom filled with isopropanol. The bottom of the container was formed by a concave glass lens with a radius of curvature of 52 mm and diameter of 50 mm. Nickel spherical particles with an average radius of 60μm and average magnetic moment $\mu = 2 \times 10^{-5}$emu (Alfa Aesar Company) were used for the experiments. The particles sedimented at the bottom of the container and were energized by a uniform uni-axial alternating magnetic field, $H = H_0 \sin(2\pi f t)$, created by a custom-built Helmoltz air-core solenoid and applied parallel to the axis of the cylindrical container. The amplitude of the AC magnetic field, H_0, was in the range of 0–75 Oe and the frequency, f, was varied from 20 to 100 Hz. For the experiments on surface spinners we used nickel spherical particles with an average size of 90 μm. About 10^3 particles were dispersed at the interface between deionized water and air. The suspension was energized by a uniform uni-axial alternating magnetic field applied parallel (in-plane) to the interface. The amplitude of the AC magnetic field was in the range of 10-60 Oe and the frequency, f, was in the range of 5-300 Hz.

The containers were mounted on a microscope stage. The trajectories of the particles were monitored by a fast CCD camera (RedLake MotionPro). We recorded image sequences (1280 x 1024 pixels resolution) at a frame-rate of 50 frames per second. Image and data analysis of the time sequences were performed by ImageJ, MatPIV and custom scripts.

V. CONCLUSION

Here we developed a high-performance computational algorithm which allowed to elucidate intricate structures of microscopic hydrodynamic flows in active colloidal systems. Our simulations faithfully reproduced experiments on colloidal rollers and spinners and provided valuable insights into the spatial organization of self-organized hydrodynamic flows. Despite the fact that the SPH is a coarse-grained approach to hydrodynamics, it provided rather accurate characterization of multi-physics colloidal systems with short and long-range interactions. With proper calibration, the approach presented here may become a predictive computational tool for a large class of systems, including active matter systems, such as Quincke rollers (colloids energized by the electric field) where the role of hydrodynamic interactions between the colloids is not clear [3, 4], and systems of elongated self-propelled particles such as microtubules or actin filaments [31, 32, 38].

ACKNOWLEDGEMENTS

The research of I.S.A., G.K. and A.S. (experiments, discrete particle modeling) was supported by the US Department of Energy, Office of Science, Basic Energy Sciences, Materials Sciences and Engineering

Division. The research of S.C. (Smoothed Particle Hydrodynamics simulations) was supported in part by the National Science Foundation under grants DMS-1613757, DMS-1311709, and DMS-1318763. The research of Y.W.(simulations) was supported in part by NSF DMS-1318763. The support by the University of Houston's Cullen Chair Funds is also acknowledged.

[1] I. S. Aranson. Active colloids. *Physics-Uspekhi*, 56(1):79, 2013.
[2] J. W. Banks, W. D. Henshaw, D. W. Schwendeman, and Q. Tang. A stable partitioned fsi algorithm for rigid bodies and incompressible flow in three dimensions. *Journal of Computational Physics*, 373:455–492, 2018.
[3] A. Bricard, J.-B. Caussin, D. Das, C. Savoie, V. Chikkadi, K. Shitara, O. Chepizhko, F. Peruani, D. Saintillan, and D. Bartolo. Emergent vortices in populations of colloidal rollers. *Nat. Commun.*, 6, 2015.
[4] A. Bricard, J.-B. Caussin, N. Desreumaux, O. Dauchot, and D. Bartolo. Emergence of macroscopic directed motion in populations of motile colloids. *Nature*, 503(7474):95–98, 2013.
[5] A. J. C. Crespo, J. M. Dominguez, A. Barreiro, and M. Gómez-Gesteira. Development of a dual cpu-gpu sph model. In *Proc 5th Int SPHERIC Workshop (Manchester)*, pages 401–407, 2010.
[6] M. Driscoll, B. Delmotte, M. Youssef, S. Sacanna, A. Donev, and P. Chaikin. Unstable fronts and motile structures formed by microrollers. *Nat. Phys.*, 13(4):375, 2017.
[7] P. Espanol and P. Warren. Statistical mechanics of dissipative particle dynamics. *EPL (Europhysics Letters)*, 30(4):191, 1995.
[8] Z. G. Feng and E. E. Michaelides. Proteus: a direct forcing method in the simulations of particulate flows. *J. Comput. Phys.*, 202:20–51, 2005.
[9] G. Gompper, T. Ihle, D. Kroll, and R. Winkler. Multi-particle collision dynamics: a particle-based mesoscale simulation approach to the hydrodynamics of complex fluids. In *Advanced computer simulation approaches for soft matter sciences III*, pages 1–87. Springer, 2009.
[10] P. Hoogerbrugge and J. Koelman. Simulating microscopic hydrodynamic phenomena with dissipative particle dynamics. *EPL (Europhysics Letters)*, 19(3):155, 1992.
[11] S. A. X. Y. Hu and N. A. Adams. A generalized wall boundary condition for smoothed particle hydrodynamics. *J. of Comp. Phys.*, 231(21):7057–7075, 2012.
[12] J. N. Israelachvili. *Intermolecular and surface forces: revised third edition*. Academic press, 2011.
[13] A. Kaiser, A. Snezhko, and I. S. Aranson. Flocking ferromagnetic colloids. *Sci. adv.*, 3(2):e1601469, 2017.
[14] T. Kempe and J. Frhlich. An improved immersed boundary method with direct forcing for the simulation of particle laden flows. *J. Comput. Phys.*, 231:3663–3684, 2012.
[15] G. Kokot, S. Das, R. G. Winkler, G. Gompper, I. S. Aranson, and A. Snezhko. Active turbulence in a gas of self-assembled spinners. *Proceedings of the National Academy of Sciences*, 114(49):12870–12875, 2017.
[16] G. Kokot, G. V. Kolmakov, I. S. Aranson, and A. Snezhko. Dynamic self-assembly and self-organized transport of magnetic micro-swimmers. *Sci. rep.*, 7(1):14726, 2017.
[17] G. Kokot, D. Piet, G. M. Whitesides, I. S. Aranson, and A. Snezhko. Emergence of reconfigurable wires and spinners via dynamic self-assembly. *Sci. Rep.*, 5, 2015.
[18] G. Kokot and A. Snezhko. Manipulation of emergent vortices in swarms of magnetic rollers. *Nat. comm.*, 9(1):2344, 2018.
[19] D. Liu, Y. Wang, W. Ma, and H. Zhang. Mesh-free gpu simulation of complex flows in three dimentional distoring domain. *Int. J. of Sci. and Inno. Math. Res.*, 3(1):6–17, 2015.
[20] G. R. Liu and M. B. Liu. *Smoothed particle hydrodynamics: a meshfree particle method*. World Scientific, 2003.
[21] M. B. Liu and G. R. Liu. Smoothed particle hydrodynamics (sph): an overview and recent developments. *Arch. of Comput. met. in eng.*, 17(1):25–76, 2010.
[22] A. Malevanets and R. Kapral. Mesoscopic model for solvent dynamics. *Jour. Chem. Phys.*, 110(17):8605–8613, 1999.
[23] J. E. Martin and A. Snezhko. Driving self-assembly and emergent dynamics in colloidal suspensions by time-dependent magnetic fields. *Rep. Prog. Phys.*, 76(12):126601, 2013.
[24] P. Maruzewski, D. L. Touzé, G. Oger, and F. Avellan. Sph high-performance computing simulations of rigid solids impacting the free-surface of water. *J. of Hydra. Res.*, 48(S1):126–134, 2010.
[25] J. J. Monaghan. Smoothed particle hydrodynamics. *Annu. rev. of astronomy and astrophysics*, 30(1):543–574, 1992.
[26] J. J. Monaghan. Simulating free surface flows with sph. *J. of Comput. phys.*, 110(2):399–406, 1994.
[27] J. J. Monaghan and A. Kocharyan. Sph simulation of multi-phase flow. *Comp. Phys. Comm.*, 87(1-2):225–235, 1995.
[28] J. P. Morris, P. J. Fox, and Y. Zhu. Modeling low reynolds number incompressible flows using sph. *J. of Comput. phys.*, 136(1):214–226, 1997.
[29] C. Moulinec, D. Emerson, X. Gu, and R. Issa. High-performance computing sph: Towards a hundred million of particle simulation. *Proc. of the 3rd SPHERIC workshop, Lausanne, Switzerland*, 2008.

[30] C. Prez, J. Pablo, G. Cervera, and J. Antonio. Efficient neighborhood search in sph. *Fluid Dynamics in Physics, Engineering and Environmental Applications Environmental Science and Engineering*, pages 185–199, 2013.
[31] T. Sanchez, D. T. Chen, S. J. DeCamp, M. Heymann, and Z. Dogic. Spontaneous motion in hierarchically assembled active matter. *Nature*, 491(7424):431–434, 2012.
[32] V. Schaller, C. Weber, C. Semmrich, E. Frey, and A. R. Bausch. Polar patterns of driven filaments. *Nature*, 467(7311):73–77, 2010.
[33] A. Snezhko and I. S. Aranson. Magnetic manipulation of self-assembled colloidal asters. *Nat. Mater.*, 10(9):698–703, 2011.
[34] A. Snezhko and I. S. Aranson. Velocity statistics of dynamic spinners in out-of-equilibrium magnetic suspensions. *Soft Matter*, 11:6055–6061, 2015.
[35] A. Snezhko, M. Belkin, I. Aranson, and W.-K. Kwok. Structure formation in electromagnetically driven granular media. *Phys. Rev. Lett.*, 102(11):118103, 2009.
[36] K. J. Solis and J. E. Martin. Complex magnetic fields breathe life into fluids. *Soft Matter*, 10(45):9136–9142, 2014.
[37] S. Succi. *The lattice Boltzmann equation: for fluid dynamics and beyond*. Oxford university press, 2001.
[38] Y. Sumino, K. H. Nagai, Y. Shitaka, D. Tanaka, K. Yoshikawa, H. Chaté, and K. Oiwa. Large-scale vortex lattice emerging from collectively moving microtubules. *Nature*, 483(7390):448–452, 2012.
[39] A. ten Cate, C. H. Nieuwstad, J. J. Derksen, and H. E. A. V. den Akker. Particle imaging velocimetry experiments and lattice-boltzmann simulations on a single sphere settling under gravity. *Physics of Fluids*, 14(11):4012–4025, 2002.
[40] B. C. van Zuiden, J. Paulose, W. T. Irvine, D. Bartolo, and V. Vitelli. Spatiotemporal order and emergent edge currents in active spinner materials. *Proc. of the National Academy of Sciences*, 113(46):12919–12924, 2016.
[41] J. Yang and F. Stern. A sharp interface direct forcing immersed boundary approach for fully resolved simulations of particulate flows. *Journal of Fluids Engineering*, 136:040904–10, 2014.
[42] S. Zhou, A. Sokolov, O. D. Lavrentovich, and I. S. Aranson. Living liquid crystals. *Proc. Natl. Acad. Sci. U.S.A*, 111(4):1265–1270, 2014.